Supporting Information

Initial Carbon–Carbon Bond Formation during the Early Stages of the Methanol-to-Olefin Process Proven by Zeolite-Trapped Acetate and Methyl Acetate

Abhishek Dutta Chowdhury[+], Klaartje Houben[+], Gareth T. Whiting, Mohamed Mokhtar, Abdullah M. Asiri, Shaeel A. Al-Thabaiti, Suliman N. Basahel, Marc Baldus,* and Bert M. Weckhuysen*

anie_201608643_sm_miscellaneous_information.pdf

S I. Experimental: Materials and Methods

All reactions and sample treatments were carried out under nitrogen atmosphere, unless specified otherwise. The H-SAPO-34, ^{12}C-methanol and ^{13}C-methanol were purchased from ACS material, Sigma Aldrich (CHROMASOLV®, for HPLC, ≥99.9%, Product number: 34860-1L-R) and Cambridge Isotope Laboratories (99 atom % [13]C, Product number: CLM-359-5), respectively. The H-SAPO-34 material under study had crystal sizes ranging mostly from 2 to 10 μm with an average particle size of 2 μm (Figure S6a-b). The Si/(Al+P) ratio is 0.21, which roughly corresponds to a theoretical amount of two Brønsted acid sites per cage.[1–3] The temperature programmed desorption of ammonia (NH$_3$-TPD) profile of H-SAPO-34, shown in Figure S6c, evidenced a combination of both weak external acid (NH$_3$-TPD lower peak temperature at around 430 K) and strong Brønsted acid (NH$_3$-TPD higher peak temperature at around 613K) sites. Ar physisorption data indicated that the H-SAPO-34 sample is mostly microporous with a BET surface area of 500 m^2/g and a micropore volume of 0.18 cm^3/g. Although this commercially available H-SAPO-34 material is already detemplated, an additional calcination has always been performed prior to the MTO reaction according to the following procedure under O$_2$ environment (flow rate of 20 mL/min): heating to 623 K at 15 K/min and keeping the sample at this temperature for the next 10 min, then heating the sample to 823 K at a rate of 5 K/min and hold there the sample for the next 90 min. Finally, the sample was cooled down to 673 K with a rate of 10 K/min under a flow of N$_2$ gas (rate of 20 mL/min).

All catalytic reactions were performed using a Linkam cell (THMS600) equipped with a temperature controller (Linkam TMS94) and its lid is equipped with a quartz window. Details of the set-up can be found in previous manuscripts from our group.[2,3] The UV-Vis diffuse reflectance spectroscopy measurements were performed with a CRAIC 20/30 PV™ UV-Vis-NIR micro-spectrophotometer using a 15X objective. A 75 W Xenon lamp was used for illumination. The on-line gas phase product analyses were performed by a Pfeiffer OmniStar GSD 320 O3 (1-300 amu) mass spectrometer (MS), which was directly connected to the outlet of the Linkam cell. The mass spectrometry database from the National Institute of Standards and Technology (NIST) was consulted for referencing purposes. Ar physisorption was performed with an automated gas sorption system Micromeritics TriStar 3000. The acidity of the samples was measured by NH$_3$-TPD using a Micrometrics AutoChem 2920 apparatus. NMR analyses were performed on the MTO reacted SAPO-34 materials using [13]CH$_3$OH. NMR experiments were performed at 11.7 T on a Bruker Avance III spectrometer equipped with a 3.2 mm magic angle spinning (MAS) probe at ambient temperature. Referencing of ^{1}H and ^{13}C chemical shifts was done externally to adamantane. An RF field of 90 kHz was used for ^{1}H hard pulses as well as SPINAL-64 decoupling and 50 kHz for ^{13}C hard pulses.[4] All spectra were processed and analyzed with Bruker Topspin3.5. 1D [1]H-^{13}C cross-polarization spectra were recorded at 10, 12 and 15 kHz MAS, used a 2s recycle delay, 16 ms acquisition time, a 50% ramp for the ^{1}H CP pulse with a 2.4 ms CP contact time and 4096 scans, except for the 15 kHz spectrum that used 2.6 ms CP contact time and 29184 scans. For the 1D ^{13}C direct excitation spectrum, a 4 s recycle delay was used, 16 ms

acquisition time and 2048 scans. All 1D spectra were processed with 25 Hz line-broadening. ^{13}C-^{13}C PDSD spectra were recorded at 12 kHz MAS, a 70% ramp for the ^1H CP pulse with a 1.6 ms CP contact time, 2 s recycle delay, 12 ms and 6 ms acquisition times for direct and indirect ^{13}C dimensions, respectively, and 30 or 150 ms for the proton-driven spin-diffusion mixing time. Spectral processing was either performed using 200 Hz line broadening in both ^{13}C dimensions, or by doubling the amount of indirect data-points through linear prediction (LP) with 32 LP coefficients and application of a 0.33*pi shifted squared sine bell window in both ^{13}C dimensions. ^{13}C-^1H proton detected CP-HETCOR spectra were recorded with an initial long ^1H-^{13}C CP of 1.6 ms and a second short ^{13}C-^1H CP of 50 or 500 μs. Both ^1H CP pulses had a ramp of 70%. Prior to the last CP, a 6 kHz MISSISSIPPI block (τ = 5 ms, N = 2) ensured destruction of on-resonance bulk ^1H magnetization.[5] A recycle delay of 2 s was used and acquisition times of 10 and 8.5 ms were used for the direct ^1H and indirect ^{13}C dimensions, respectively. Spectral procession was either performed using only 1 ms of the ^{13}C indirect dimension and applying 100 Hz line-broadening to both dimensions, or by applying a 0,33*pi shifted squared sine bell window.

The MTO reactions were performed without any pressing and sieving the H-SAPO-34 catalyst. In each case, ~ 30 mg of the catalyst material were used. Initially it was placed on the heating stage of Linkam cell, which was further connected to water cooler. The inlet of the reactor was connected to the N_2 gas line, via a methanol saturator, whereas outlet is either connected to the Pfeiffer mass spectrometer or vented out. The lid of the Linkam cell is equipped with a quartz window to monitor the reaction by UV-Vis diffuse reflectance spectroscopy. Prior to each UV-Vis diffuse reflectance spectroscopy measurement, the H-SAPO-34 material was calcined according to the procedure described above. Then, a N_2 flow of 20 mL/min was introduced at 673 K to a saturator with methanol. The UV-Vis diffuse reflectance spectra were recorded every 30 s interval during the MTO experiment, which typically took 60 min. After a 30 min or 60 min of reaction time, the reaction was quenched by rapid cooling of the Linkam cell by using Linkam TMS94 temperature controller. The same procedure was also followed during the control reaction using methyl acetate (instead of methanol).

S II. Additional Long-Term Experiment

In an effort to further understand the mechanism of the MTO process we have stored the ^{13}C-enriched NMR sample for 6 months and subsequently investigated the material with ssNMR. Figure S7 compares the ^1H-^{13}C CP ssNMR spectra of a freshly reacted and a 6-month stored H-SAPO-34 exposed to the MTO reaction at 673 K. It was found that the 6-month storage led to an increase in the amount of aromatics with a simultaneous decrease in the amounts of DMM, methanol and DME. This observation could be attributed to the higher reactivity, higher mobility and lower stability of DMM, methanol and DME. Indeed, the conversion of DMM into aromatics over zeolite-based materials is well-established.[6,7] The relatively broader peak of DMM and methanediol (compared to methanol or DME) suggest its plausible interaction with the zeolite framework. It could further be rationalized on the basis of the different decomposition rate
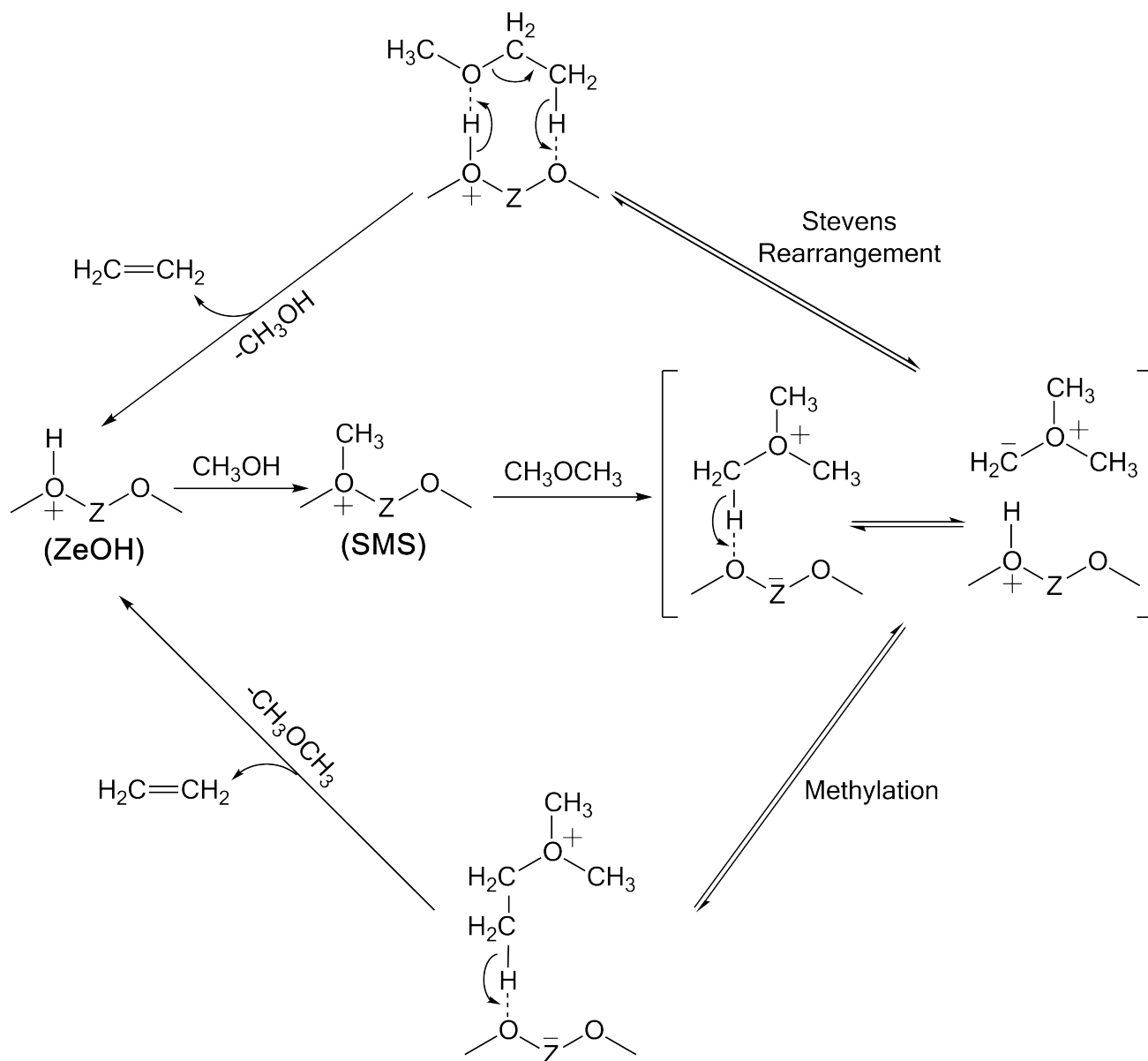
of DMM anomers, in the 6-months stored sample (Figures 2d & S7). Interestingly, a ~2:1 ratio of two DMM anomers was observed in the fresh sample, whereas it was ~ 1:1 in the 6-month stored sample.

## S III. Control Experiment with Methyl Acetate

In order to gain further mechanistic information on the induction period, as well as to understand the fate of methyl acetate during the MTO reaction, an additional control experiment was performed using *operando* UV-Vis diffuse reflectance spectroscopy (DRS) with online mass spectrometry (MS), with methyl acetate as an effluent instead of methanol under identical experimental conditions. The results of this control experiment are summarized in Figure S8, which appeared to be similar to the MTO reaction (as shown in Figures S2 and S3). Figure S8a reveals spectral features during the first 10 min of reaction, as absorption bands at ~297, 350, 419, 483 and 630 nm increase in intensity as a function of reaction time (Figure S8c). Just like the MTO reaction, a decrease in intensity was observed in the case of the 630 nm band after an initial ~7 min of reaction, which could be attributed to the existence of intra-molecular transformation within the zeolite framework (see the main manuscript for the in-depth discussion and assignment of these bands). In general, these band positions and their time dependent behavior were quite similar to the MTO reaction, as shown in Figures S2 & S3. The only notable spectroscopic difference (compared to MTO reaction) was the absence of a 387 nm band in the case of methyl acetate as an effluent, which belongs to the hexamethylbenzenium ion. Thus, methyl acetate was able to generate the hydrocarbon pool species upon exposure to H-SAPO-34 at 673K. Next, the MS data of this reaction, as presented in Figure S8d, reveals the presence of methane, methanol, dimethyl ether (DME), lower olefins (ethylene, propylene and traces of butylene) and dimethoxymethane (DMM). Therefore, the detection of methanol/DME from methyl acetate implies the transformation between methanol and methyl acetate is actually reversible (path c in Scheme 1) over zeolite at 673K. Interestingly, a substantial quantity of DMM was observed from methyl acetate (Figure S8d), whereas only traces of DMM were detected during the MTO reaction (Figure S2d). It could be due to the presence of a higher amount of *in-situ* formed carbon monoxide (*i.e.* decarbonylation of methyl acetate), which facilitates the transformation to surface formate species from H-SAPO-34 *via* "Koch-type" carbonylation reaction (see Scheme S2).

In essence, (like methanol) methyl acetate is itself capable of producing lower olefins and initiating the hydrocarbon pool mechanism. Therefore, it is safe to assume that surface acetate and methyl acetate could be regarded as the influential 'methanol-derived' intermediates during the induction period of the MTO reaction. Moreover, it also provides justification in support of the *microscopic reversibility* of path c in Scheme 1 and the mechanism of formation of surface formate species as well (Scheme S2).

S IV. Scheme

Scheme S1. Plausible catalytic cycle of the MTO reaction comprising of the "direct mechanism" for the first C-C bond formation (see Scheme 1) and the well-established "hydrocarbon pool" mechanism (this scheme). The reaction products and intermediates indicated in blue have been experimentally observed in this work, whereas other reaction intermediates have already been either theoretically verified or experimentally evidenced in the open literature.[7–13]

Scheme S2. The schematic illustration of the oxonium ylide mechanism. Herein, the dimethyl ether is proposed to react with either surface methoxy species (SMS) or protonated methanol ($CH_3OH_2^+$) over Brønsted acid sites of the zeolite to form a trimethyl oxonium ion or dimethyl oxonium methyl ylide (via additional proton abstraction). Then, it undergoes either an intramolecular Stevens rearrangement or an intermolecular methylation. Both pathways eventually lead to the formation of ethylene via β-elimination. This oxonium ylide mechanism was very well reviewed by Stöcker et al.[14] and Olsbye et al.[8] It should be noted that, although our NMR data is consistent with the formation of SMS and dimethylether (57 and 52 ppm, respectively), all other proposed intermediates were not observed fully by our NMR experiments. The oxonium ylide species could be partially compatible with the 52/57 ppm correlation, but no correlation is observed between methoxy and ylide carbon. The proposed intermediate through the methylation pathway (bottom cycle) could be compatible with 52/57 ppm, but again, no 57-CH_3 correlation is observed. Similarly, CH_2CH_3 correlation is missing in support of the proposed intermediate through the Stevens rearrangement (top cycle).
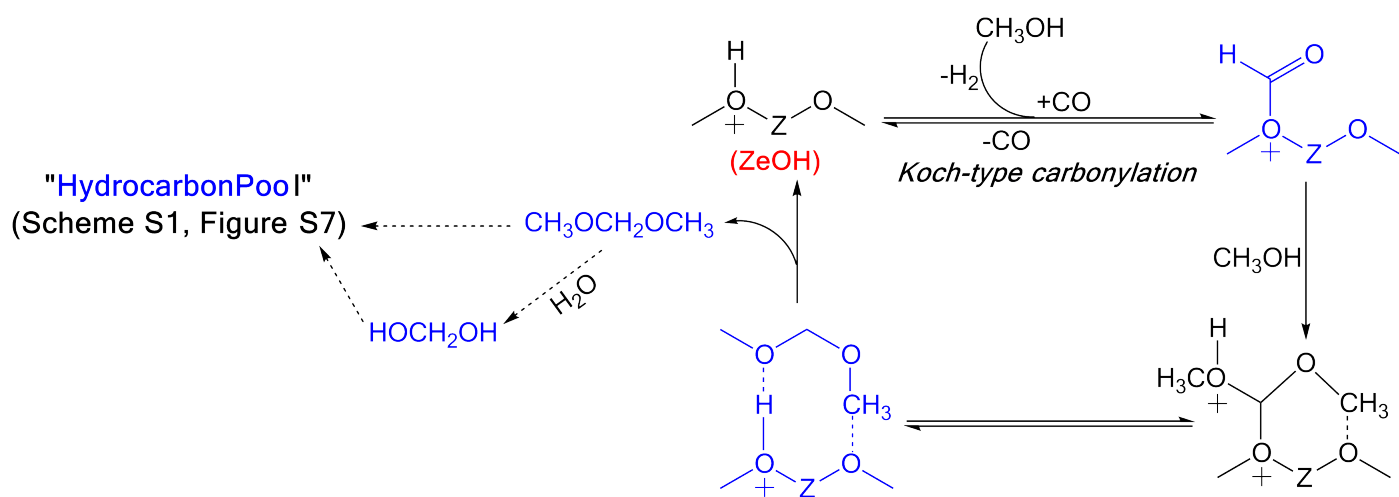
Scheme S3. Plausible mechanistic route to the formation of surface formate species, dimethoxymethane (DMM) and methanediol during H-SAPO-34-catalyzed Methanol-to-Olefin (MTO) reaction. Their spectroscopic signatures are illustrated in Figures 2 and 3 in the manuscript. The reaction products and intermediates indicated in blue have been experimentally observed in this work.

S V. Figures
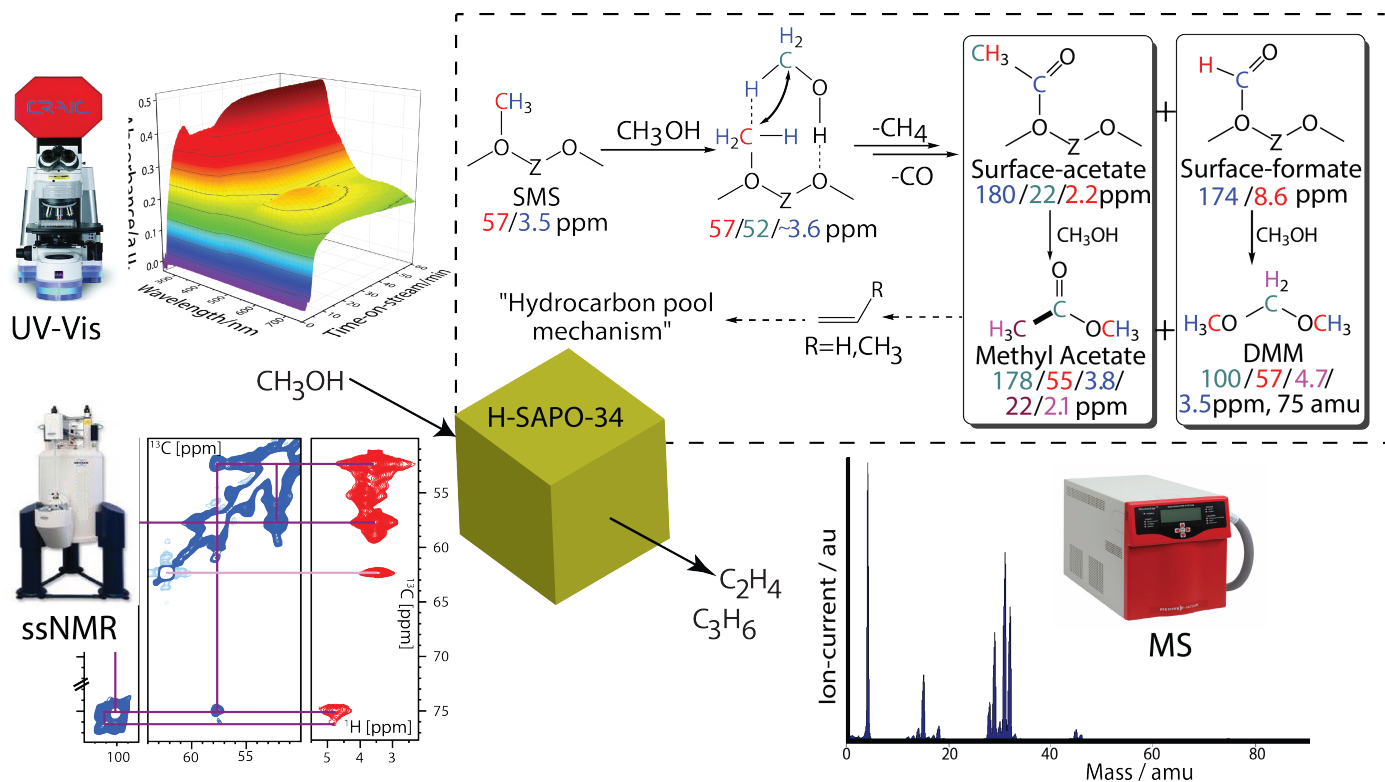
Figure S1. Schematic of the spectroscopic approach taken to investigate the early stages of the H-SAPO-34-catalyzed Methanol-to-Olefin (MTO) reaction using *operando* UV-Vis diffuse reflectance spectroscopy coupled with on-line mass spectrometry (MS) and *ex-situ* magic angle spinning solid-state nuclear magnetic resonance (MAS ssNMR). The initial stages of the MTO reaction, consisting of the formation of surface formate/acetate, methyl acetate and dimethoxymethane (DMM) from surface methoxy species (SMS), are shown, including the ^{1}H and ^{13}C ssNMR fingerprints.
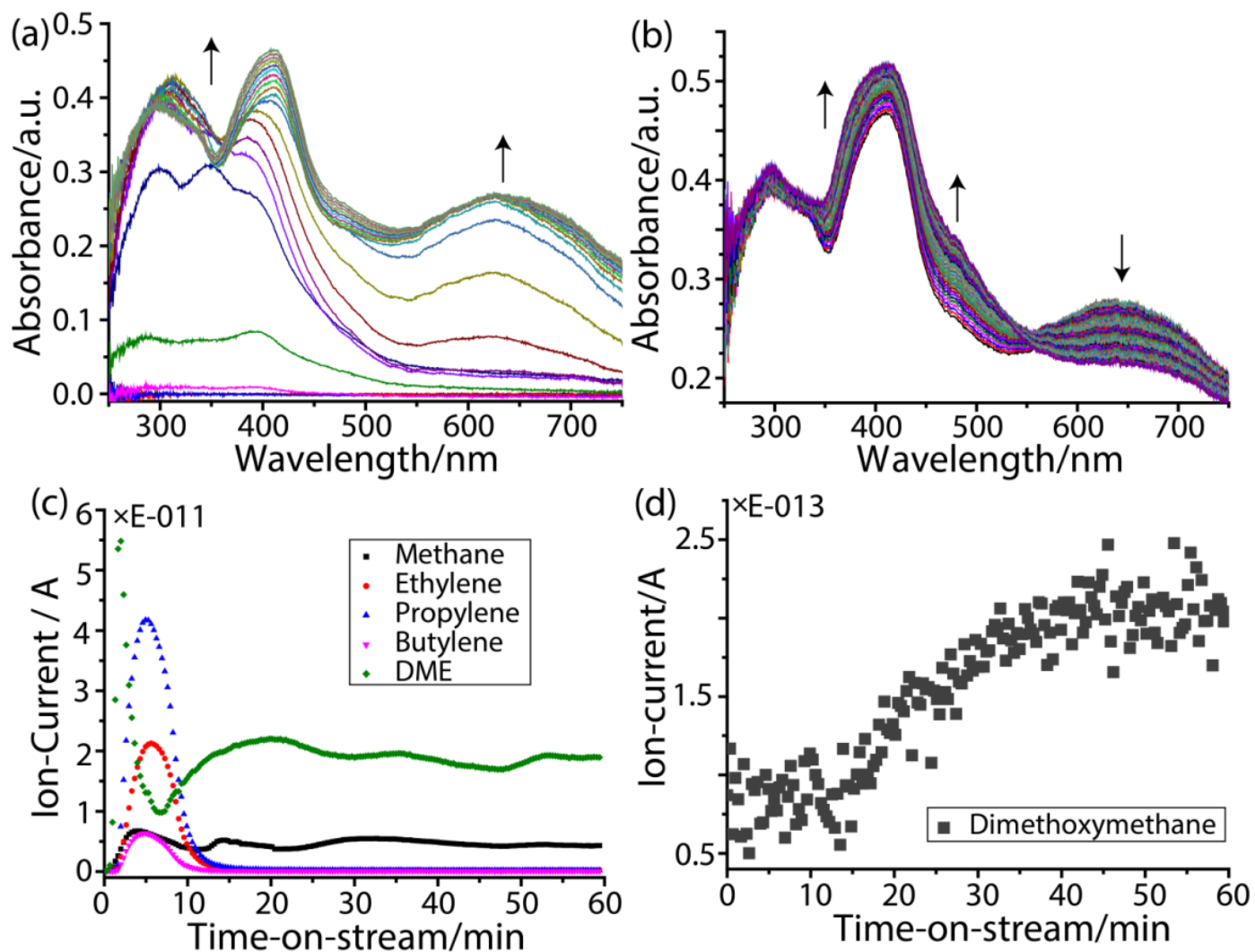
Figure S2. *Operando* UV-Vis diffuse reflectance spectra of H-SAPO-34 being exposed for (a) 0-10 min and (b) 10-60 min to the Methanol-to-Olefin (MTO) reaction at 673 K and (c, d) the mass spectra (MS) profiles for methane, ethylene, propylene, butylene, dimethyl ether (DME) and dimethoxymethane (DMM) as a function of reaction time.
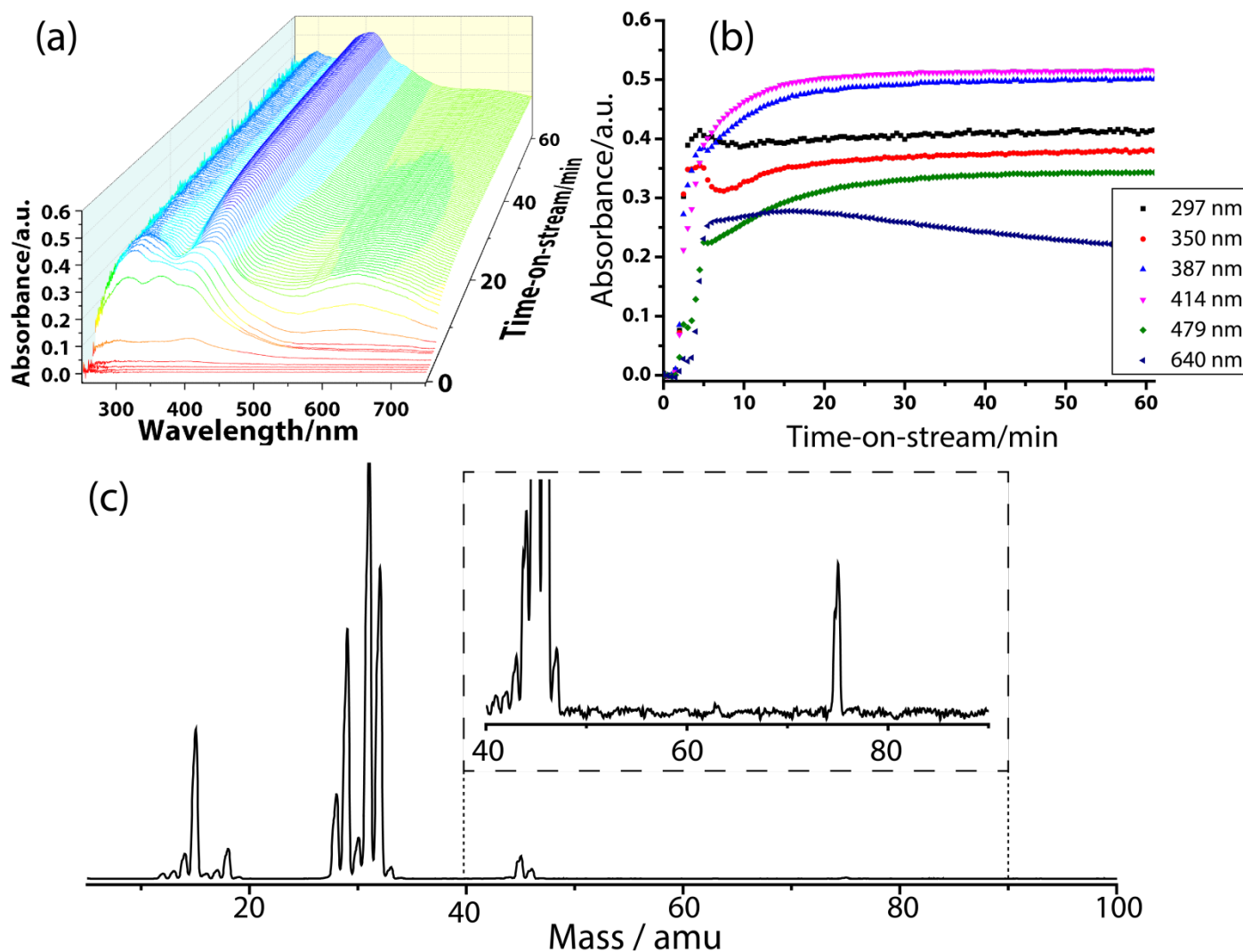
Figure S3. The time-dependent *operando* UV-Vis diffuse reflectance spectroscopy measurements during the MTO reaction conducted at 673 K over H-SAPO-34 for 60 min: (a) 3D plot of the UV-Vis diffuse reflectance spectra as a function of reaction time. (b) Change of the absorbance as a function of reaction time. (c) Representative mass spectrum where m/z=75 exclusively belongs to DMM, while its 100% relative abundance peak at m/z=45 is overlapping with a peak originating from DME.
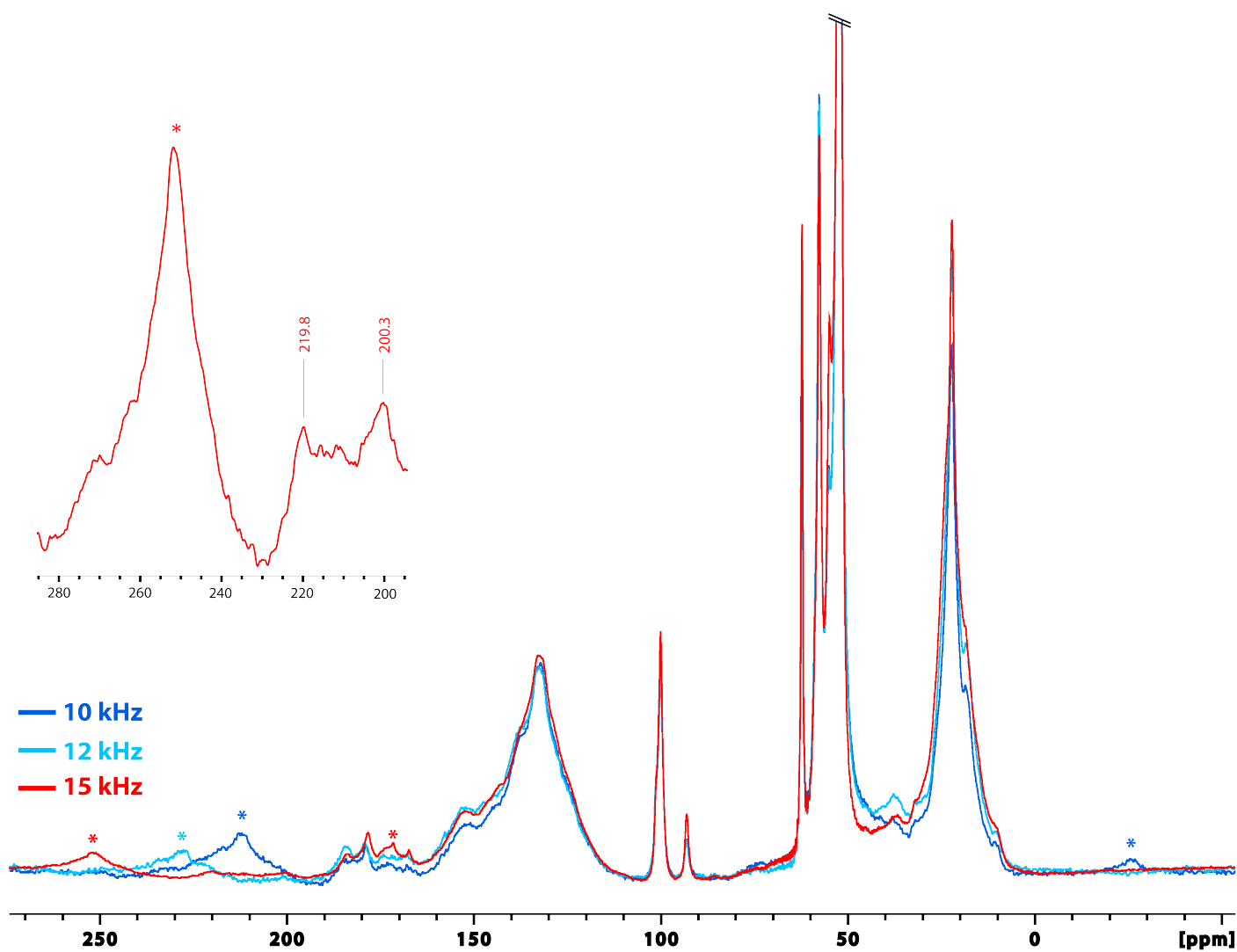
Figure S4. 1D ^{1}H-^{13}C CP MAS NMR spectra of H-SAPO-34 exposed to the MTO reaction with ^{13}C-MeOH at 673 K for 30 min.
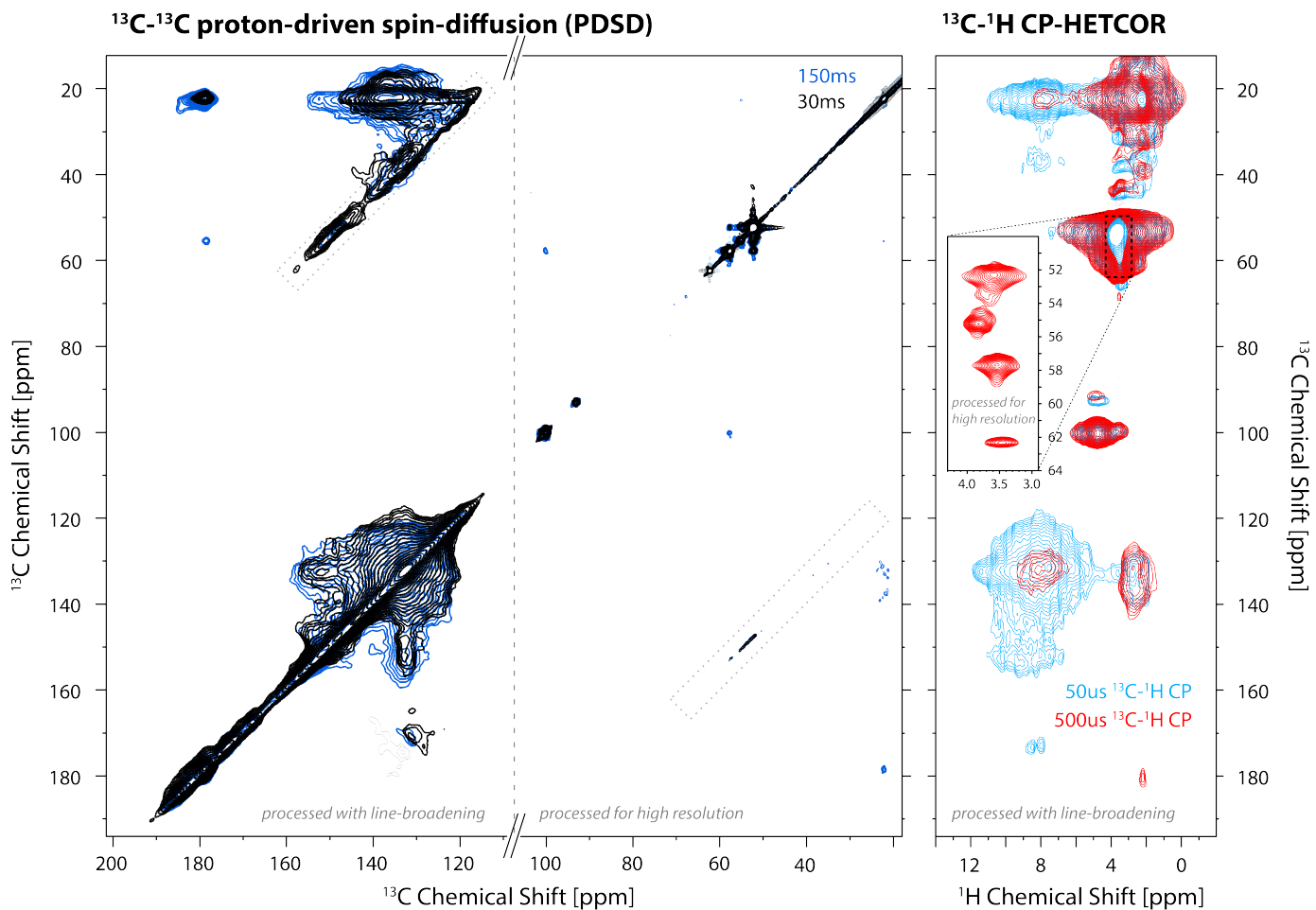
Figure S5: 2D ^{13}C proton-driven spin-diffusion spectra and ^{13}C-^{1}H proton detected CP-HETCOR spectra of H-SAPO-34 exposed to the MTO reaction with ^{13}C-MeOH at 673 K for 30 min. Processing details are mentioned in the experimental section. Gray dashed boxes indicate spinning side bands.
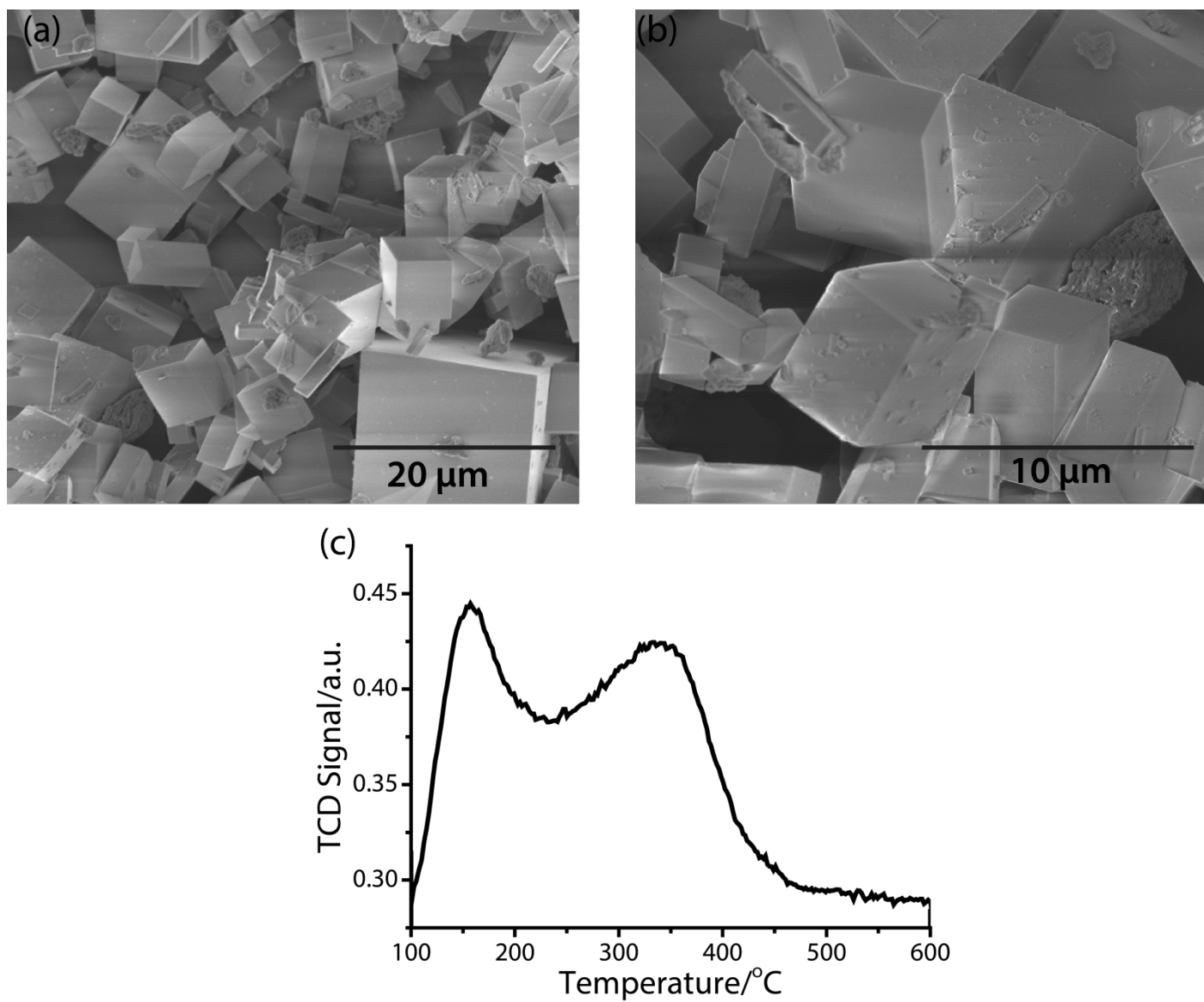
Figure S6. (a, b) Representative SEM images and (c) the NH$_3$-TPD profile of the fresh H-SAPO-34 catalyst used in this study.
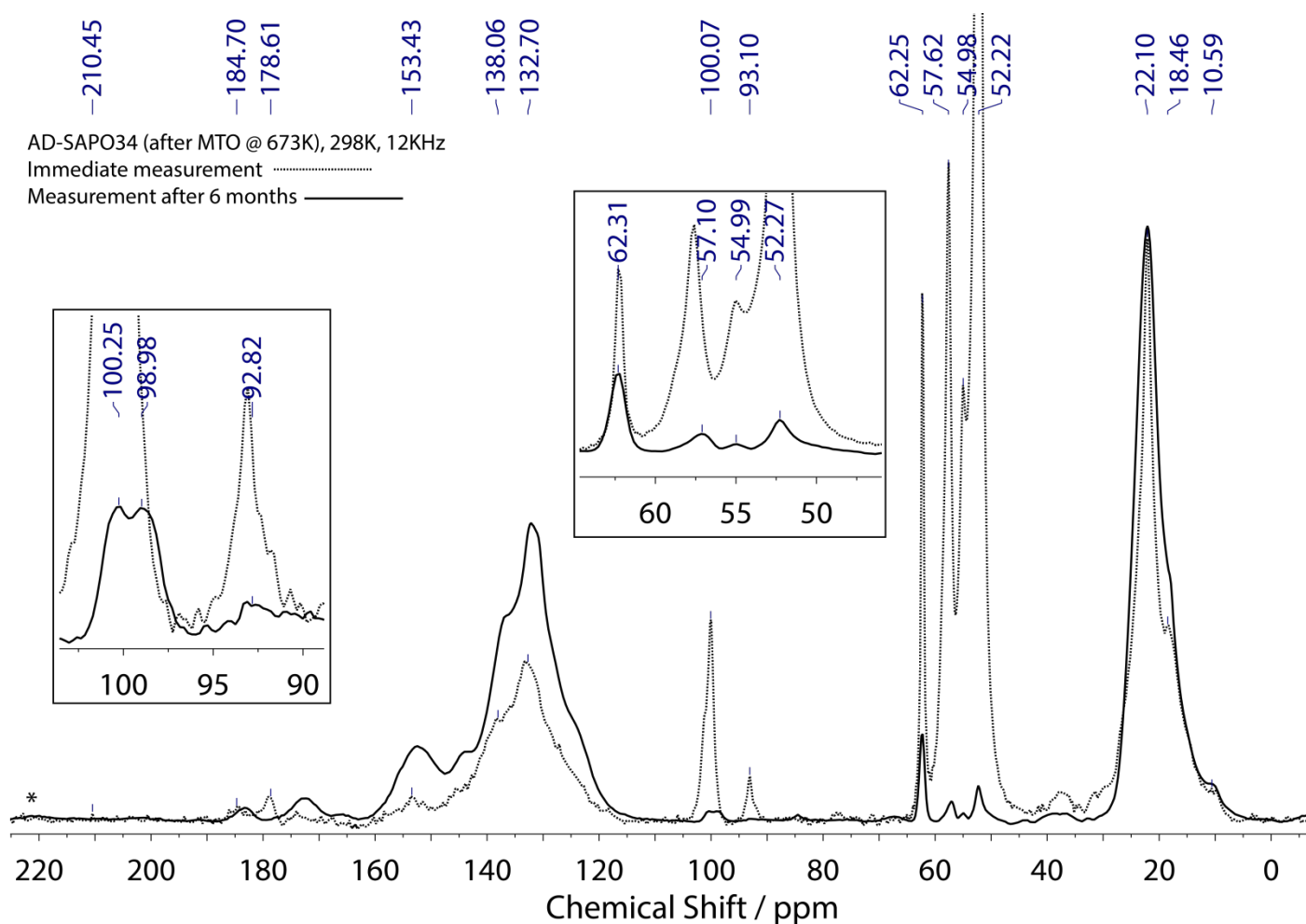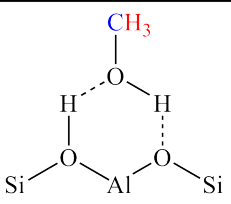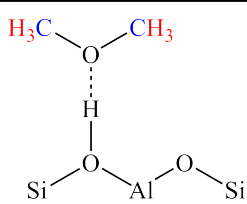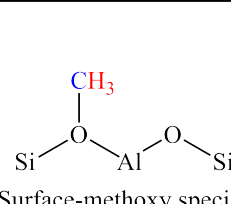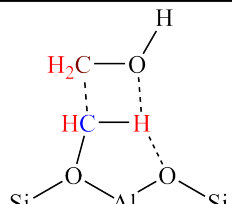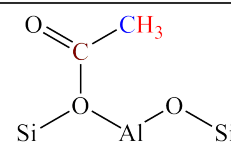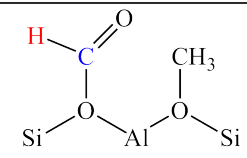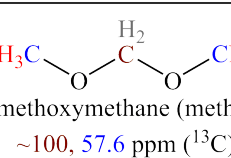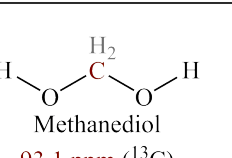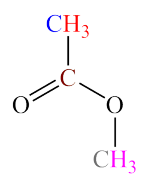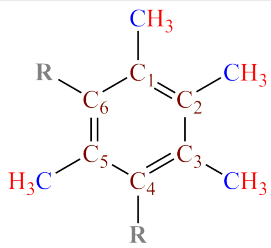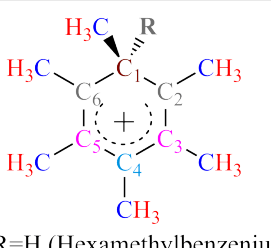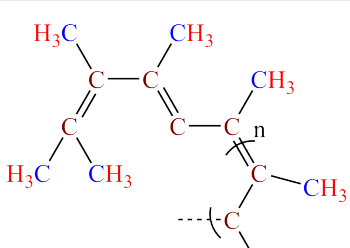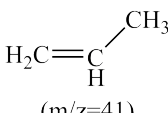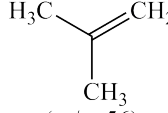
Figure S7. The ^{1}H-^{13}C CP MAS NMR spectra of H-SAPO-34 exposed to the MTO reaction at 673 K for 30 min. The catalyst sample was measured immediately (⋯⋯) and after 6 months (—). The spectra were scaled at 22.1 ppm in order to make comparison possible.
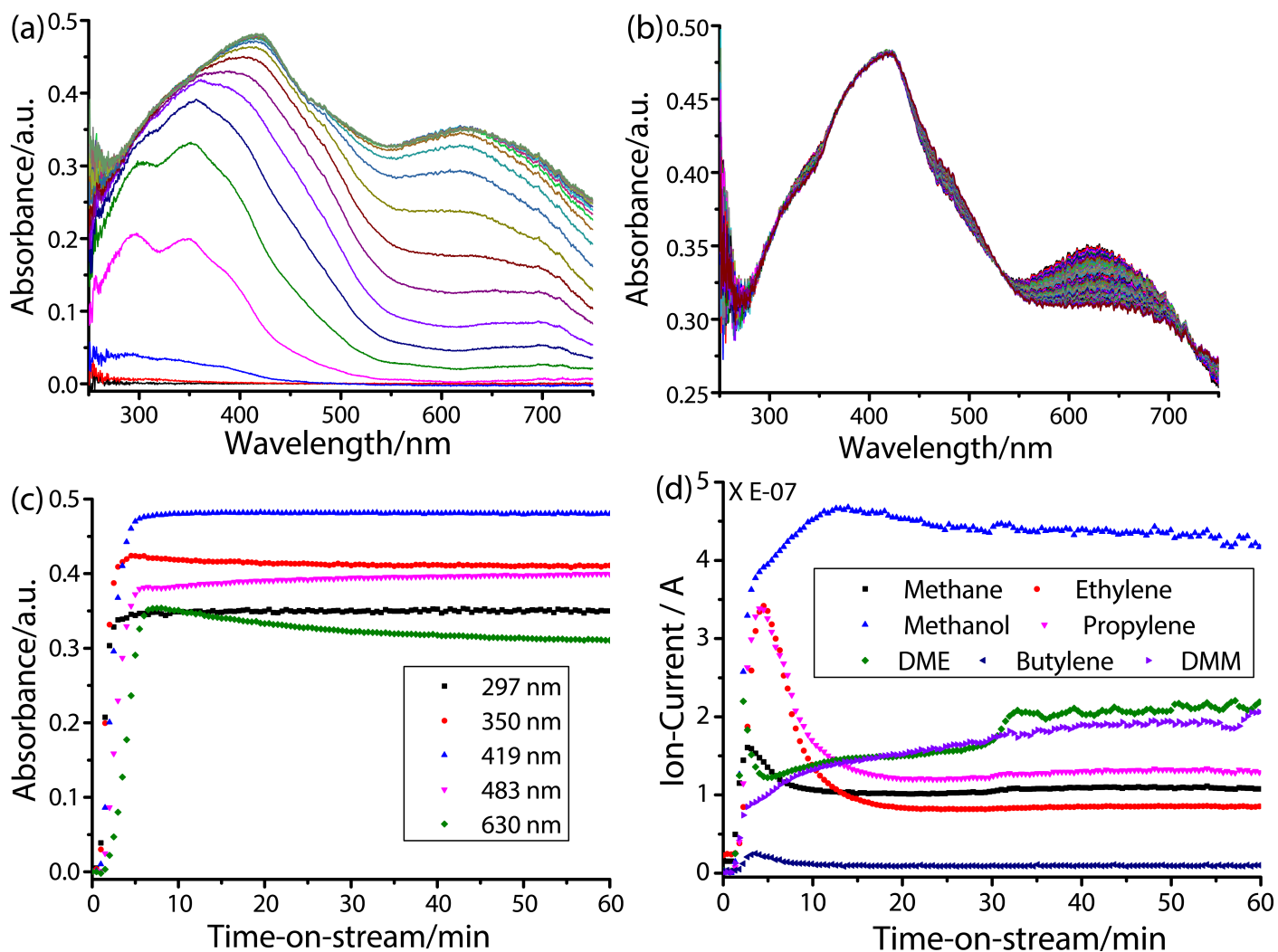
Figure S8. *Operando* UV-Vis diffuse reflectance spectra of H-SAPO-34 being exposed for (a) 0-10 min and (b) 10-60 min to the methyl acetate at 673 K. (c) Change of the absorbance as a function of reaction time and (d) the mass spectra (MS) profile for methane, ethylene, methanol, propylene, butylene, dimethyl ether (DME) and dimethoxymethane (DMM) as a function of reaction time.

S VI. Table

Table S1. Overview of the reaction intermediates and products, including their spectroscopic fingerprints, observed in this work.

 Methanol 52.2 ppm (^{13}C) 3.6 ppm (^{1}H) m/z=**31**, 32	 Dimethylether (*side-on*) 62.2 ppm (^{13}C) 3.5 ppm (^{1}H) m/z=**45**, 46	 Surface-<u>methoxy</u> species 57.6 ppm (^{13}C) 3.5 ppm (^{1}H)	 Adduct of Surface-methoxy species and methanol 57.6, 52.2 ppm (^{13}C) 3.5-3.6 ppm (^{1}H)
 Surface-<u>acetate</u> species 180.5, 22.2 ppm (^{13}C) 2.2 ppm (^{1}H)	 Surface-<u>formate</u> species 173 ppm (^{13}C) 8.6 ppm (^{1}H)	 Dimethoxymethane (methylal) ~100, 57.6 ppm (^{13}C) 4.7, 3.5 ppm (^{1}H) m/z=**45**,75	 Methanediol 93.1 ppm (^{13}C) 4.9 ppm (^{1}H) m/z=**31**
 Methyl Acetate 178.5, 55.2, 22.2 ppm (^{13}C) 2.2, 3.82 ppm (^{1}H)	 R=H (tetramethylbenzene), CH$_3$ (Hexamethylbenzene) 18-22, 132.2 (if R=CH$_3$), 128-138 (if R=H) ppm (^{13}C) 2.1-2.2 ppm (^{1}H), 7.0-7.2 ppm (^{1}H, if R=H) λ (nm)=284-297 nm	 R=H (Hexamethylbenzenium), CH$_3$ (Heptamethylbenzenium) ~22, 55, 132-145, 178-185, 201-210 ppm (^{13}C) 2.2 ppm (^{1}H), **3.8 ppm** (^{1}H, if R=H) λ (nm)=387-414 nm	 methylated conjugated poly-ene(-yl) species 15-27, 131-154 ppm (^{13}C) 1-1.8 ppm (^{1}H) λ (nm)=300-350 nm
Following additional species were observed by MS in gas-phase during MTO			
CH$_4$ (m/z=16)	H$_2$C=CH$_2$ (m/z=26)	 (m/z=41)	 (m/z=56)

S VII. References

[1]   L. R. Aramburo, J. Ruiz-Martínez, L. Sommer, B. Arstad, R. Buitrago-Sierra, A. Sepúlveda-Escribano, H. W. Zandbergen, U. Olsbye, F. M. F. deGroot, B. M. Weckhuysen, *ChemCatChem* **2013**, *5*, 1386–1394.

[2]   Q. Qian, C. Vogt, M. Mokhtar, A. M. Asiri, S. A. Al-Thabaiti, S. N. Basahel, J. Ruiz-Martínez, B. M. Weckhuysen, *ChemCatChem* **2014**, *6*, 3396 – 3408.

[3]   Q. Qian, D. Mores, J. Kornatowski, B. M. Weckhuysen, *Microporous Mesoporous Mater.* **2011**, *146*, 28–35.

[4]   B. M. Fung, A. K. Khitrin, K. Ermolaev, *J. Magn. Reson.* **2000**, *142*, 97–101.

[5]   D. H. Zhou, C. M. Rienstra, *J. Magn. Reson.* **2008**, *192*, 167–172.

[6]   Y. Fu, H. Zhu, J. Shen, *Thermochim. Acta* **2005**, *434*, 88–92.

[7]   Y. Liu, S. Müller, D. Berger, J. Jelic, K. Reuter, M. Tonigold, M. Sanchez-Sanchez, J. A. Lercher, *Angew. Chemie Int. Ed.* **2016**, *55*, 5723–5726.

[8]   U. Olsbye, S. Svelle, K. P. Lillerud, Z. H. Wei, Y. Y. Chen, J. F. Li, J. G. Wang, W. B. Fan, *Chem. Soc. Rev.* **2015**, *44*, 7155–7176.

[9]   P. Tian, Y. Wei, M. Ye, Z. Liu, *ACS Catal.* **2015**, *5*, 1922–1938.

[10]   S. Ilias, A. Bhan, *ACS Catal.* **2013**, *3*, 18–31.

[11]   D. Lesthaeghe, V. Van Speybroeck, G. B. Marin, M. Waroquier, *Ind. Eng. Chem. Res.* **2007**, *46*, 8832–8838.

[12]   S. R. Blaszkowski, R. A. van Santen, *J. Am. Chem. Soc.* **1997**, *119*, 5020–5027.

[13]   A. Comas-Vives, M. Valla, C. Copéret, P. Sautet, *ACS Cent. Sci.* **2015**, *1*, 313–319.

[14]   M. Stöcker, *Microporous Mesoporous Mater.* **1999**, *29*, 3–48.